Contrib Mineral Petrol (1993) 114:395–408

Contributions to Mineralogy and Petrology

Granulite xenoliths from western Saudi Arabia: the lower crust of the late Precambrian Arabian-Nubian Shield

Anne V. McGuire [1] **and Robert J. Stern** [2]

[1] Department of Geosciences, University of Houston, Houston, TX 77204-5503, USA
[2] Center for Lithospheric Studies, University of Texas at Dallas, Richardson, TX 75083-0688, USA

Received August 17, 1992 / Accepted February 26, 1993

Abstract. Mafic and intermediate granulite xenoliths, collected from Cenozoic alkali basalts, provide samples of the lower crust in western Saudi Arabia. The xenoliths are metaigneous two-pyroxene and garnet granulites. Mineral and whole rock compositions are inconsistent with origin from Red Sea rift-related basalts, and are compatible with origin from island arc calc-alkaline and low-potassium tholeiitic basalts. Most of the samples are either cumulates from mafic magmas or are restites remaining after partial melting of intermediate rocks and extraction of a felsic liquid. Initial $^{87}Sr/^{86}Sr$ ratios are less than 0.7032, except for two samples at 0.7049. The Sm–Nd data yield T_{DM} model ages of 0.64 to 1.02 Ga, similar to typical Arabian-Nubian Shield upper continental crust. The isotopic data indicate that the granulites formed from mantle-derived magmas with little or no contamination by older continent crust. Calculated temperatures and pressures of last reequilibration of the xenoliths show that they are derived from the lower crust. Calculated depths of origin and calculated seismic velocities for the xenoliths are in excellent agreement with the crustal structure model of Gettings et al. (1986) based on geophysical data from western Saudi Arabia. Estimation of mean lower crustal composition, using the granulite xenoliths and the Gettings et al. (1986) crustal model, suggests a remarkably homogeneous mafic lower crust, and an andesite or basaltic andesite bulk composition for Pan-African juvenile continental crust.

Introduction

Obtaining a better understanding of the generation and evolution of the Earth's continental crust is a primary goal of a large group of earth scientists. Many models have been developed to explain how such crust forms and how this process has varied with time. The paradigm is that the continental crust formed by amalgamation of primitive arc terranes of andesitic composition which subsequently underwent internal differentiation (e.g., Taylor 1967). Unfortunately, our knowledge of the composition and evolution of the upper continental crust is far superior to our understanding of the lower crust, limiting our ability to infer the bulk composition of continental crust and therefore evaluate models for its generation and internal differentiation.

The crust of NE Africa and Arabia is extremely well exposed and provides a remarkable opportunity to examine processes of crust formation. The Arabian-Nubian Shield (ANS) formed during the late Precambrian "Pan-African" event (ca. 900–550 Ma). With the exception of the Afif terrane of south-central Arabia, the basement east of the Nile is derived either directly from the mantle or via remelting of mantle-derived rocks, as inferred from Sr and Nd isotopic systematics (Harris et al. 1990). Numerous ophiolite-decorated suture zones can be identified leading to the acceptance of the terrane model of arc accretion for the formation of Afro-Arabian crust (Stoeser and Camp 1985; Vail 1985; and others). The ANS is one of the best preserved and exposed examples of juvenile continental crust, and understanding its evolution will illuminate these processes of continental crustal formation.

This paper presents data for the first time on the composition of the lower crust as inferred from xenoliths recovered from five widely separated alkali basalt fields erupted through late Precambrian crust in western Saudi Arabia (Fig. 1). Available geophysical data (Gettings et al. 1986) from the region allow us better to evaluate the extent to which the xenoliths are representative of the lower crust in the region. We feel that these results are particularly important because the continental crust of the Arabian-Nubian Shield formed by juvenile addition from the mantle to the crust, as a result of processes indistinguishable from modern plate tectonics. Correspondingly, understanding the composition and evolution of the ANS lower crust is important to our understanding of lithospheric evolution.

Correspondence to: A.V. McGuire

Previous work

The majority of previous work has been mineralogical and geochemical studies of mafic, metaigneous granulite xenoliths from Israel (Esperança and Garfunkel 1986; Mittlefehldt 1983, 1986) and Algeria (Leyreloup et al. 1982). Leyreloup et al. (1982) studied lower crustal metaigneous and metasedimentary granulite xenoliths from Hoggar in southern Algeria. The Hoggar basalts are erupted through Precambrian crust which was reactivated during the Pan-African orogeny, and the Hoggar granulites may be Pan-African or older in age. To our knowledge, almost nothing has been published on the granulite xenoliths of Saudi Arabia. Henjes-Kunst et al. (1990) report Sr- and Nd-isotopic data for one granulite xenolith from Harrat Lunayyir (Fig. 1) in western Saudi Arabia.

Outcrops of ANS lower crust are found only on Zabargad Island in the Red Sea, where it was exposed during incipient rifting of the Red Sea. Felsic granulites yield Rb–Sr and Sm–Nd ages of 650–700 Ma, interpreted to date peak metamorphism; mafic granulites yield a Sm–Nd mineral age of ca. 550 Ma, interpreted as the time of amphibolite-facies retrogression (Lancelot and Bosch 1991). The petrology and geochemistry of these rocks has been studied by Bonatti and Seyler (1987), Seyler and Bonatti (1988), Boudier et al. (1988), and Lancelot and Bosch (1991).

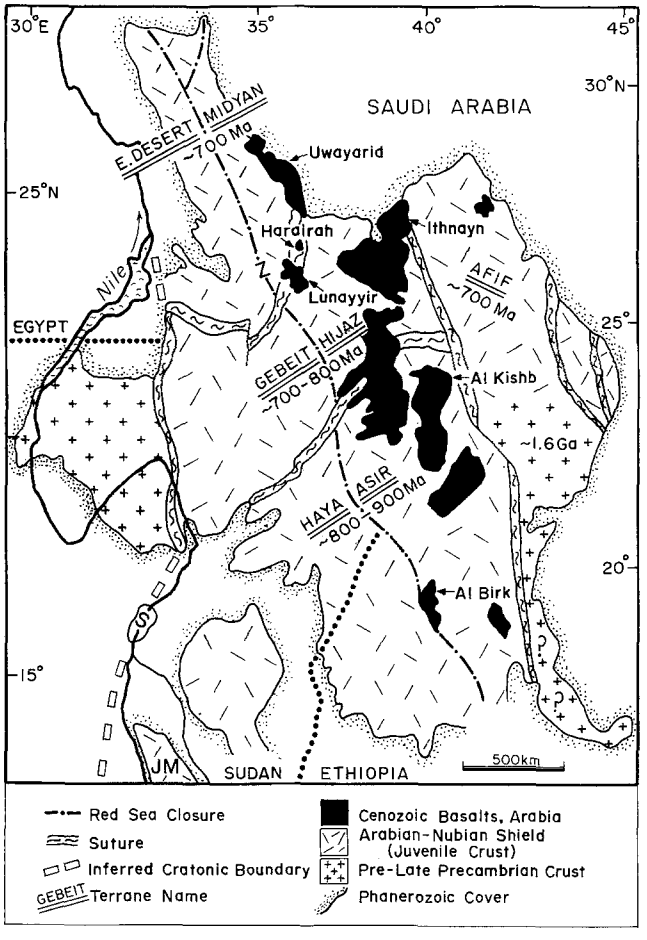

Fig. 1. Map of the Arabian-Nubian Shield, with the Red Sea closed (modified after Abdelsalam and Stern 1992). Localities of alkali basalt fields yielding lower crustal xenoliths used in this paper are shown. Names of terranes are *double underlined*. Approximate ages of terranes are given. Approximate location of the boundary between the juvenile terranes of the Arabian-Nubian Shield and those of the pre-late Precambrian "Nile Craton" is shown as a *dashed line*. Other occurrences of lower crustal rocks in the region include Jebel Moya, *JM*; Sabaloka, *S*; and Zabargad Island, *Z*

Sample description

The twenty samples selected for study represent all the inclusions with greater than 5 modal percent plagioclase, with no evidence of host basalt infiltration, and size greater than $3 \times 3 \times 3$ cm, from a large (>1,000 samples) suite of xenoliths collected by Robert G. Coleman in conjunction with U.S. Geological Survey studies of western Saudi Arabia. This xenolith collection is presently curated by the National Museum of Natural Sciences, Smithsonian Institution. The only other plagioclase-bearing xenoliths in this suite are mantle pyroxenites containing small amounts of plagioclase resulting from breakdown of garnet (McGuire 1988). Granulite xenolith sizes ranged from 3 cm to about 10 cm diameters.

The samples were collected with mantle xenoliths from Red Sea rift-related basalt flows and cinder cones in five basalt fields in western Saudi Arabia (Fig. 1). These localities are separated by as much as 1,000 km (Fig. 1), and lie on different Precambrian crustal terranes (Fig. 1). Harrat al Birk was erupted on the southern 800–900 Ma Asir terrane; whereas Harrat al Kishb sits on the 700–800 Ma northern part of the Asir terrane. Harrat Ithnayn overlies the 700–800 Ma Hijaz terrane. Harrat Uwayrid overlies the younger 600–700 Ma Midyan terrane and may overlap southward onto the Yanbu suture zone between the Midyan and Hijaz terranes. Harrat Harairah was erupted through the Yanbu suture zone.

The majority of xenoliths studied (17 out of 20) are two-pyroxene granulites consisting of plagioclase, clinopyroxene, orthopyroxene, opaques (ilmenite, magnetite), and various accessory phases such as apatite, rutile, zircon, and biotite. Two textures occur in these rocks: Fine- to medium-grained samples are generally equigranular, with granoblastic texture, and many exhibit foliation defined by tabular pyroxene grains. In some samples there is compositional layering with thin (<2 mm) clinopyroxene-rich and orthopyroxene-rich bands. Orthopyroxene is strongly pleochroic. Clinopyroxene typically exsolves ilmenite. Modal plagioclase is generally 70–80%, with equal amounts of clinopyroxene and orthopyroxene. This type of granulite occurs at Harrat Uwayrid, Harrat Ithnayn, Harrat Harairah, and Harrat al Birk. Other two-pyroxene granulite samples are unfoliated medium- to coarse-grained, equigranular, with allotriomorphic-granular or hypidiomorphic-granular texture. Abundances of clinopyroxene are greater than orthopyroxene and modal plagioclase is generally less than 50%. This type of granulite occurs at Harrat al Kishb, Harrat Ithnayn, and Harrat al Birk.

One two-pyroxene granulite sample (93413-A1, Harrat al Birk) consists of medium-grained, anhedral clinopyroxene + plagioclase, and fine-grained patches of clinopyroxene + orthopyroxene + plagioclase + spinel. The textures of these patches are similar to textures described by Ghent et al. (1980) and McGuire (1988) in pyroxenite xenoliths from the same locality and attributed to breakdown of garnet under conditions of decreasing pressure or increasing temperature during crustal thinning and heating associated with Red Sea rifting.

Three of the xenoliths are garnet bearing (10–30 modal percent) with plagioclase + clinopyroxene ± orthopyroxene and accessory (<1%) ilmenite, rutile, or spinel. All are from the Harrat al Birk locality. The rocks are medium grained, inequigranular, with granoblastic or allotriomorphic-granular textures. Clinopyroxene is zoned, but not exsolved. One xenolith (93754) exhibits compositional banding with alternating plagioclase-rich and pyroxene-garnet-rich layers. Sample 93413-B2 shows corona texture in the form of fine-grained, vermicular-textured orthopyroxene + plagioclase + spinel rims on garnet. The rims are most pronounced at garnet-clinopyroxene grain contacts. In all three garnet-bearing samples, formerly euhedral to subhedral garnets are now cryptocrystalline aggregates of orthopyroxene + plagioclase + spinel ± olivine ± clinopyroxene formed by decompression breakdown reactions during transport of the xenoliths in their host basalts.

Analytical methods

Mineral compositions were determined by using a JEOL 733 automated electron microprobe at Stanford University (15 kV acceleration voltage, 15 nA beam current, 10 μm defocused beam, 30 s count times) and a JEOL 8600 Superprobe at the University of Houston (UH) (15 kV acceleration voltage, 20 nA beam current, focused beam, 40 s count times except 20 s on Na). Analyses were run on the cryptocrystalline "garnet" aggregates using a beam defocused to 50 μm diameter to determine bulk garnet compositions. Stanford analyses used the BA matrix correction of Albee and Ray (1970), and UH analyses used a Tracor Northern ZAF correction routine. Representative mineral compositions are reported in Tables 1–4. Errors are approximately ±1–2 relative percent on major elements and ±5–10 relative percent on minor elements.

Two samples (H353-A, H332-7) were too small for whole rock analysis. For the larger samples, weathering and basalt rinds were removed by sawing. The samples were crushed and powdered in a tungsten-carbide shatterbox (ring mill). Whole rock rare earth, trace and major elements were analyzed by inductively-coupled plasma spectroscopy (ICP) at the University of Houston using a Thermo Jarrell Ash ICP spectrometer and methods described in Norman et al. (1989). Four replicate counts were collected for each element in each sample. Working curves were constructed using a minimum of six USGS rock standards for each analysis run. Concentrations in samples were computed using these curves. Results are given in Tables 5, 6. Analytical errors are ±1–5 relative percent for major elements, ±5–10 relative percent for trace elements and ±1–5 relative percent for rare-earth elements (REE), based on standard deviation of replicate counts and replicate analyses of USGS standards.

Nickel, Cr, Ga, and Pb values were determined on whole rocks powders using standard X-ray fluorescence (XRF) spectroscopy at Stanford University and Washington State University. Relative errors are ±10%.

Isotopic analyses of Sr and Nd were performed at the University of Texas, Dallas using a Finnigan MAT 261 mass spectrometer. All samples were dissolved for one week in Krogh bombs (Krogh 1973) to ensure dissolution of minor refractory phases. Thirty-three analyses of the E and A $SrCO_3$ during the course of this work yielded a mean $^{87}Sr/^{86}Sr = 0.70801$. In-run precision was smaller than the long-term reproducibility of the standard (±0.0004) and the latter is accepted here as the analytical uncertainty. All samples are normalized to $^{87}Sr/^{86}Sr = 0.70800$ for the E and A standard. The Rb and Sr contents were determined by isotope dilution.

Chemical procedures for Nd follow those of Lin et al. (1989, 1990). Analytical details of the $^{143}Nd/^{144}Nd$ determinations are reported by Stern et al. (1990). Calculations of ε-Nd were made assuming Bulk Earth $^{147}Sm/^{144}Nd = 0.1967$ and using the determinations of ε-Nd for the UCSD standard (−15.2) and BCR (−0.16) reported by Pier et al. (1989) to calculate a Bulk Earth $^{143}Nd/^{144}Nd$ appropriate for the UTD laboratory (UCSD Nd $^{143}Nd/^{144}Nd = 0.511829$ and BCR = 0.512606); the total range of ±0.000020 obtained for the standards is taken to be the analytical uncertainty for this work. Total processing blanks for Sr and Nd were less than 2 ng and 0.5 ng, respectively, and are negligible relative to typical dissolutions of ca. 70 μg Sr and 1.5 μg Nd.

Results

Mineral compositions

There are no systematic geographic variations in mineral compositions. Mineral compositions are homogeneous in most of the xenoliths; however, several samples demonstrate zoning in plagioclase and pyroxenes. Plagioclase is oligoclase to labradorite (An_{27-57}) (Fig. 2; Table 1). Where present, plagioclase zoning is normal with 1–6% anorthite variation. Calcic pyroxenes are augites (Fig. 2; Table 2) with variable atomic Mg/(Mg+∑Fe) (Mg #) of 0.59–0.80. Five samples exhibit slight concentric zoning; however, zonation is highly variable from one sample to the next. Low-Ca pyroxenes are hypersthenes (CaO contents <1.25 wt%) with variable Mg # from 0.46 to 0.80. Alumina contents are less than 3 wt% for most orthopyroxenes (Table 3).

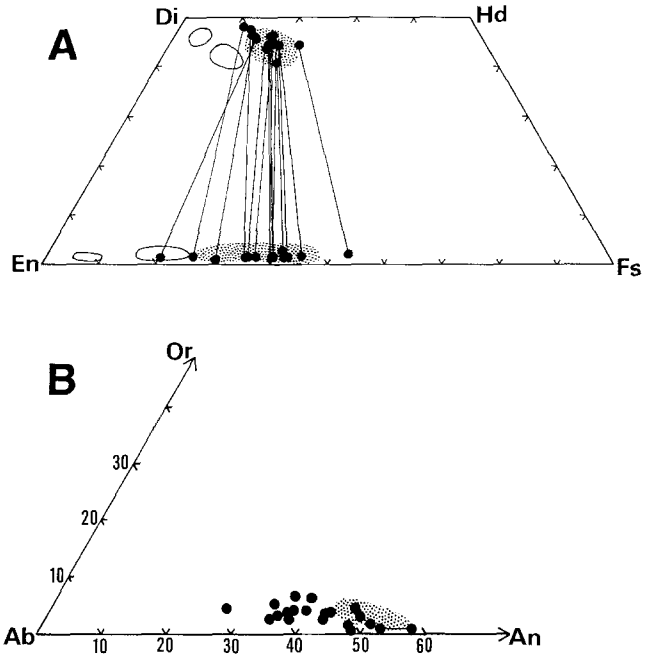

Fig. 2. Granulite pyroxene (**A**) and plagioclase (**B**) compositions, *filled dots. Circled fields* are compositions from Saudi Arabian mantle xenoliths (McGuire 1988); *stippled fields* are compositions from Hoggar metaigneous granulites (Leyreloup et al. 1982)

Garnet compositions were determined by defocused beam microprobe analyses on the three garnet granulite xenoliths. Analyses presented in Table 4 are the averages of 10 analysis spots for each sample. The three compositions are similar and are approximately PYR_{45} ALM_{40} GRO_{15}. Low Na_2O (0.08–0.36 wt%) in the analyses suggests only minor alteration of the original garnet bulk composition during the breakdown reaction.

Three iron-titanium oxide assemblages are observed. Several samples contain near-endmember ilmenite and no other Fe–Ti oxide phases. Other samples contain an ilmenite-hematite solid solution phase and a magnetite-ulvöspinel solid solution. Some granulite xenoliths contain rutile+ilmenite+hematite with varying degrees of ilmenite and hematite solid solution. Aluminous spinel is observed in only two xenoliths and is a breakdown product of garnet.

Whole rock compositions

Whole rock compositions are presented in Tables 5 and 6. The two-pyroxene granulites are either hypersthene normative or slightly nepheline normative, and the gar-

Table 1. Representative granulite plagioclase compositions

Sample no.	H310-23	H310-24	H332-18	H353-B	H353-1	H353-34	H30-82-54	93413-A1	93712	93719
SiO_2	57.4	59.6	58.1	59.2	57.2	55.6	61.1	55.6	58.5	56.3
Al_2O_3	27.4	25.8	25.9	25.4	27.6	27.6	24.3	29.3	25.9	27.9
FeO	0.1	0.2	0.2	0.1	0.2	0.2	0.1	0.0	0.4	0.1
MgO	0.0	0.0	0.0	0.0	0.0	0.0	0.0	0.0	0.0	0.0
CaO	9.1	7.5	8.2	7.2	9.6	9.9	5.6	10.8	8.6	10.0
Na_2O	5.4	5.7	6.4	7.2	5.4	5.8	7.8	5.2	6.0	5.5
K_2O	0.3	1.0	0.7	0.5	0.8	0.1	0.8	0.2	0.4	0.5
Total	99.7	99.8	99.5	99.6	100.8	99.2	99.7	101.1	99.8	100.3

Table 2. Representative clinopyroxene compositions

Sample no.	H310-23	H310-25	H332-7	H353-A	H353-34	H30-82-54	93754	93413-B2	93488-A2	93712
SiO_2	49.4	50.5	51.0	51.9	51.4	50.7	52.4	49.1	50.7	51.0
Al_2O_3	6.7	4.1	4.2	2.6	5.0	5.4	4.4	8.0	2.8	3.5
FeO	9.8	11.1	9.7	13.3	8.5	8.0	6.0	8.4	12.4	10.3
MgO	11.5	12.1	11.9	10.7	12.7	12.5	14.2	12.6	12.8	13.2
MnO	0.2	0.3	0.2	0.3	0.1	0.1	0.2	0.2	0.3	0.2
TiO_2	0.6	0.4	0.5	0.3	0.5	0.8	0.8	1.2	0.5	0.4
Cr_2O_3	0.1	0.1	0.1	0.0	0.0	0.1	0.3	0.1	0.1	0.1
CaO	20.4	20.1	20.6	20.1	20.1	20.8	21.4	18.9	18.8	20.4
Na_2O	1.2	1.0	0.9	0.6	1.2	1.6	1.0	1.3	0.7	0.7
Total	99.9	99.7	99.1	99.8	99.5	100.0	100.7	99.8	99.1	99.8

Table 3. Representative orthopyroxene compositions

Sample no.	H310-23	H310-25	H332-7	H353-A	H353-1	H30-82-54	93413-B2	93488-A2	93712	93754
SiO_2	50.9	50.7	52.1	51.8	50.7	52.9	50.8	51.1	51.5	54.5
Al_2O_3	4.7	2.5	2.5	1.0	1.9	2.9	6.3	1.7	1.8	2.6
FeO	22.8	25.0	24.6	31.6	27.9	19.2	18.0	25.5	22.4	16.3
MgO	21.5	20.6	20.6	15.2	18.7	24.9	23.7	20.0	22.5	25.9
MnO	0.5	0.6	0.5	0.6	0.6	0.3	0.4	0.5	0.5	0.3
TiO_2	0.1	0.1	0.1	0.1	0.1	0.1	0.3	0.2	0.1	0.2
Cr_2O_3	0.0	0.0	0.1	0.0	0.0	0.1	0.0	0.1	0.0	0.1
CaO	0.6	0.7	0.6	0.9	0.7	0.4	1.2	1.3	0.8	0.7
Na_2O	0.0	0.0	0.1	0.0	0.0	0.0	0.1	0.0	0.0	0.1
Total	101.1	100.2	101.2	101.2	100.6	100.8	100.8	100.4	99.6	100.7

Table 4. Garnet compositions. Each is average of ten defocused beam microprobe analyses

Sample no.	93413-B2	93751-B	93754
SiO_2	40.4	41.0	40.9
Al_2O_3	22.5	23.8	23.7
FeO	17.5	17.7	16.7
MgO	12.6	9.5	11.4
MnO	0.5	0.4	0.7
TiO_2	0.2	0.2	0.2
Cr_2O_3	0.0	0.1	0.1
CaO	6.2	7.4	5.6
Na_2O	0.1	0.3	0.4
Total	100.0	100.4	99.7

net granulites are hypersthene normative (CIPW norm calculated using wt% $Fe_2O_3/FeO = 0.15$). None of the samples exhibit normative quartz or corundum that is characteristic of metasedimentary or felsic metaigneous rocks. The granulites are mafic to slightly intermediate in composition with 43 to 57 wt% SiO_2. They are generally aluminum rich; 11 out of 18 have Al_2O_3 in the range 17–20 wt%, but none are as aluminous as metasediments. Potassium contents are low (less than 0.9 wt% K_2O). There is a wide range of Mg #, from 0.40 to 0.76. There are no systematic variations in whole rock composition relative to xenolith locality.

There is a great deal of scatter in the trace element compositions (Fig. 3). The lack of element correlations,

Table 5. Whole rock major element compositions

Sample no.	Two-pyroxene granulite								
Locality	H30-82-54 Al Kishb	H332-18 Harairah	H353-B Ithnayn	H353-1 Ithnayn	H353-33 Ithnayn	H353-34 Ithnayn	H310-23 Uwayrid	H310-24 Uwayrid	H310-25 Uwayrid
SiO_2	48.7	52.9	51.4	53.7	44.5	46.1	49.6	55.4	56.6
TiO_2	0.7	0.9	1.9	0.4	2.7	2.1	0.6	0.4	0.4
Al_2O_3	18.9	17.9	19.6	18.2	17.1	14.3	16.3	17.6	18.0
FeO	8.0	9.2	6.1	7.4	14.3	13.5	7.8	6.5	6.8
MnO	0.2	0.2	0.1	0.1	0.2	0.2	0.1	0.1	0.1
MgO	7.5	5.2	3.1	5.6	5.4	9.3	6.4	5.3	5.5
CaO	11.2	9.8	7.7	9.6	10.2	10.7	12.3	9.3	8.3
Na_2O	3.3	4.0	5.5	3.9	2.7	2.1	3.5	4.4	4.6
K_2O	0.4	0.5	0.4	0.6	0.2	0.1	0.2	0.8	0.9
P_2O_5	0.4	0.3	0.4	0.0	0.4	0.2	0.1	0.1	0.1
Total	99.3	100.2	96.2	99.5	97.7	98.6	96.9	99.9	101.3
Mg #	0.63	0.50	0.47	0.58	0.40	0.55	0.59	0.59	0.59

Sample no.	Two-pyroxene granulite						Garnet granulite		
Locality	93413-A1 Al Birk	93427 Al Birk	93488-A2 Al Birk	93712 Al Birk	93719 Al Birk	93751-A Al Birk	93413-B2 Al Birk	93751-B Al Birk	93754 Al Birk
SiO_2	43.0	51.2	54.9	52.8	50.3	47.9	51.6	45.0	50.6
TiO_2	0.6	0.5	0.8	0.6	0.6	1.5	1.2	0.4	0.8
Al_2O_3	16.6	7.7	19.5	18.1	15.1	17.3	11.1	17.3	15.6
FeO	13.7	8.2	5.9	7.4	6.5	13.6	8.2	12.4	8.1
MnO	0.3	0.2	0.1	0.1	0.1	0.1	0.1	0.3	0.2
MgO	9.4	14.4	3.8	6.5	6.5	6.7	9.4	9.2	8.8
CaO	12.2	13.0	6.6	9.2	16.2	6.3	12.6	10.4	8.9
Na_2O	1.5	1.5	5.3	3.6	2.3	2.9	3.2	1.4	3.4
K_2O	0.0	0.1	0.6	0.2	0.3	0.5	0.2	0.2	0.4
P_2O_5	0.1	0.1	0.3	0.1	0.1	0.2	0.0	0.1	0.1
Total	97.4	96.9	97.8	98.6	98.0	97.0	97.6	96.7	96.9
Mg #	0.55	0.76	0.53	0.61	0.64	0.47	0.67	0.57	0.66

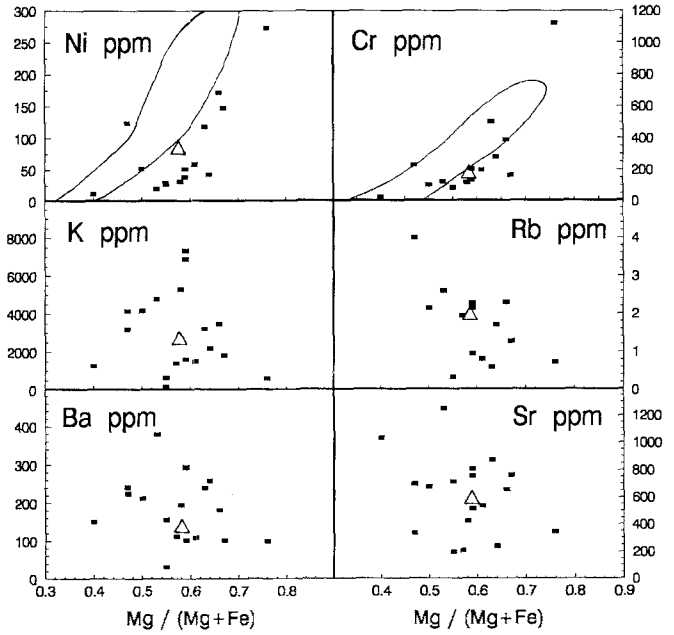

Fig. 3. Trace element contents versus atomic Mg # [Mg/(Mg+$\sum$Fe)]. *Triangles* mark average granulite composition. Compositional fields of Arabian alkali basalts (Camp and Roobol 1989) are outlined on Ni and Cr plots

and the distances between the various xenoliths localities (up to 1,000 km), suggests that these samples should not be treated as a co-magmatic suite. There is a positive correlation of compatible trace elements (Ni, Cr) with Mg # and a rough negative correlation of some highly incompatible trace elements (Ba, K, Rb) with Mg # (Fig. 3). Other trace elements (Sr, Sc, Y, Zr, V, Ti, REE) scatter widely and do not correlate with Mg # or SiO_2. Trace element ratios are extremely variable. Very high K/Rb (539–5355) reflects the very low Rb contents. High Ba and Sr contents are reflected in low K/Ba (4–27) and Rb/Sr (0.0007–0.012), and high Ba/La (16–205) and Sr/Nd (27–227). The REE patterns range from light-rare-earth-element (LREE)-enriched to one LREE-depleted sample (Fig. 4): chondrite-normalized $(La/Yb)_n$ ranges from 0.3 to 11.1. Positive and negative Eu anomalies are observed (Eu/Eu* 0.6–2.0).

Isotopic compositions

The present $^{87}Sr/^{86}Sr$ measured for 18 samples ranges from 0.70291 to 0.70522 (Table 7). The very low $^{87}Rb/^{86}Sr$ (<0.035) in these rocks results in the calculated

Table 6. Whole rock trace and rare earth element compositions (ppm)

Sample no.	Two-pyroxene granulite								
	H30-82-54	H332-18	H353-B	H353-1H353-33	H353-34	H310-23	H310-24	H310-25	
Sc	29	26	10	27	29	33	38	16	19
V	270	220	190	200	470	460	250	130	140
Cr	500	100	NA	120	25	88	NA	200	140
Ni	120	52	NA	32	12	27	NA	52	39
Cu	55	20	50	13	16	24	25	9	7
Zn	110	100	72	69	130	120	66	69	75
Ga		19		15					
Rb	0.60	2.15	1.12	5.0	0.35	0.76	0.95	2.14	2.27
Sr	870	680	700	420	1030	720	510	800	760
Y	10	24	12	17	11	9	18	11	15
Zr	84	75	57	39	29	25	35	16	24
Ba	240	210	230	200	150	160	100	300	300
Pb	NA	2	NA	ND	NA	NA	NA	NA	NA
La	12	13	8.8	5.5	4.0	2.8	2.5	2.3	1.4
Ce	32	31	21	13	12	9.4	8.1	4.6	4.6
Nd	23	19	14	8.4	11	8.1	7.0	3.6	3.3
Sm	5.0	4.3	3.2	2.3	3.0	2.3	2.3	1.4	1.6
Eu	1.8	1.5	1.3	1.2	0.9	1.0	0.5	0.7	0.8
Gd	4.0	4.3	2.9	2.5	2.9	2.2	2.7	1.8	2.0
Yb	0.7	2.1	0.8	1.6	0.8	0.8	1.7	1.0	1.5
K/Rb	5360	1940	2850	1060	3640	860	1720	3230	3240
Sm/Nd	0.22	0.22	0.23	0.27	0.27	0.29	0.33	0.40	0.49
Sr/Nd	38	35	49	50	95	89	73	220	230
Ba/La	20	17	26	36	38	56	41	125	205
$(La/Yb)_n$	11	4.1	7.0	2.4	3.3	2.5	1.0	1.5	0.7

ND, none detected

Table 6 (continued)

Sample no.	Two-pyroxene granulite						Garnet granulite		
	93413-A1	93427	93488-A2	93217	93719	93751-A	93413-B2	93751-B	93754
Sc	51	47	13	27	33	34	26	48	21
V	420	250	120	190	240	320	230	230	300
Cr	84	1120	130	200	280	230	170	NA	390
Ni	30	270	20	59	43	120	150	NA	170
Cu	46	26	87	25	18	74	85	22	53
Zn	110	88	83	100	99	120	51	110	64
Ga	15	11				20			15
Rb	0.33	0.74	2.60	0.81	1.71	4.00	1.28	1.93	2.30
Sr	200	350	1250	540	240	340	770	210	660
Y	38	13	9	20	14	21	19	14	11
Zr	77	48	32	66	44	130	26	50	30
Ba	32	99	380	110	260	240	100	110	180
Pb	ND	ND	NA	NA	NA	ND	NA	NA	1
La	1.5	4.7	10	5.9	5.0	7.5	2.4	3.2	3.9
Ce	6.5	15	23	16	13	19	6.7	10	12
Nd	7.1	13	14	12	8.2	12	4.4	7.6	9.5
Sm	3.2	3.3	3.0	3.2	2.3	3.2	1.9	2.2	2.8
Eu	0.8	0.9	1.8	0.8	0.8	1.2	0.8	0.9	1.3
Gd	5.2	3.2	2.3	3.4	2.6	3.7	2.3	2.1	2.5
Yb	3.7	1.1	0.7	1.9	1.1	1.9	1.8	1.4	1.0
K/Rb	540	850	1840	1870	1280	1040	1430	740	1510
Sm/Nd	0.46	0.25	0.21	0.27	0.28	0.27	0.43	0.29	0.29
Sr/Nd	28	27	89	45	29	29	173	27	69
Ba/La	21	21	38	19	52	32	43	35	47
$(La/Yb)_n$	0.3	3.0	9.2	2.1	3.0	2.7	0.9	1.6	2.7

ND, none detected
NA, not analysed

Table 7. Granulite Sr and Nd isotopic compositions

	$^{87}Rb/^{86}Sr$	$^{87}Sr/^{86}Sr$	$^{87}Sr/^{86}Sr_{(750\ Ma)}$	$^{147}Sm/^{144}Nd$	$^{143}Nd/^{144}Nd$	T_{DM}(Ga)	ε-$Nd_{(750\ Ma)}$
Harrat al Kishb							
H30-82-54	0.0021	0.70293	0.70291	0.131	0.51266	0.68	7.2
Harrat Harairah							
H332-18	0.0089	0.70307	0.70297	0.134	0.51260	0.81	5.8
Harrat Ithnayn							
H353-B	0.0045	0.70316	0.70311	0.137	0.51265	0.74	6.5
H353-1	0.032	0.70291	0.70257	0.166	0.51279	0.74	6.5
H353-33	0.00094	0.70323	0.70322	0.166	0.51272	0.97	5.0
H353-34	0.0032	0.70335	0.70332	0.172	0.51274	1.02	4.9
Harrat Uwayrid							
H310-23	0.0055	0.70309	0.70303	0.199	0.51292	0.99	5.9
H310-24	0.0072	0.70302	0.70294	NA	NA	NA	NA
H310-25	0.0083	0.70305	0.70296	0.297	0.51316	0.22	1.1
Harrat al Birk							
93413-A1	0.0058	0.70309	0.70303	0.275	0.51316	0.20	3.1
93427	0.0058	0.70296	0.70290	0.153	0.51272	0.76	6.3
93488-A2	0.0062	0.70302	0.70295	0.129	0.51257	0.81	5.8
93719	0.208	0.70510	0.70488	0.171	0.51278	0.84	5.9
93712	0.0044	0.70294	0.70289	0.164	0.51283	0.64	7.2
93751-A	0.034	0.70522	0.70485	0.165	0.51274	0.88	5.6
93413-B2	0.0047	0.70305	0.70300	0.261	0.51303	−0.06	2.1
93751-B	0.026	0.70347	0.70320	0.174	0.51279	0.87	5.7
93754	0.0101	0.70332	0.70321	0.178	0.51274	1.18	4.3

NA, not analysed

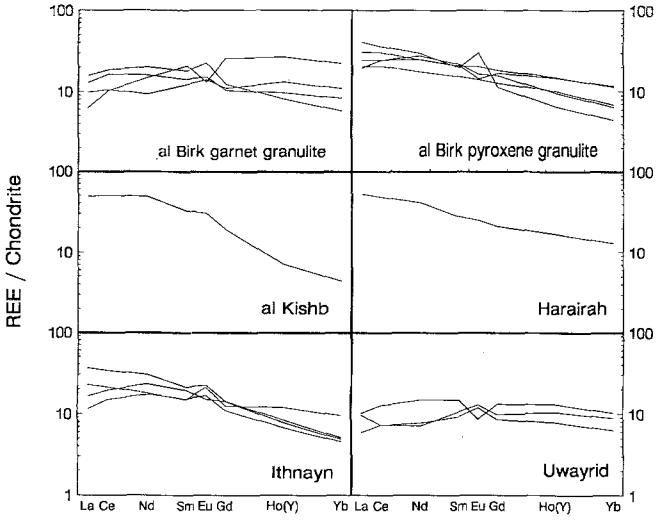

Fig. 4. Chondrite-normalized REE patterns for the Arabian granulite xenoliths

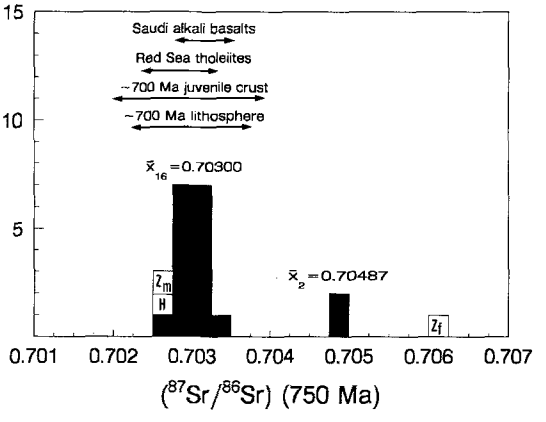

Fig. 5. Inferred initial $^{87}Sr/^{86}Sr$ for granulite xenoliths compared with ranges observed in possible cogenetic suites. Ranges for Red Sea rift alkali and tholeiitic basalts (Altherr et al. 1990), Arabian lithosphere estimated from mantle xenoliths (Henjes-Kunst et al. 1990), and ca. 700 Ma juvenile Arabian upper crust (Stern and Kröner 1992) are shown. H_j, value for one granulite xenolith from Henjes-Kunst et al. (1990); Z_m, mafic granulite and Z_f, felsic granulite from Zabargad Island, Lancelot and Bosch (1991)

initial $^{87}Sr/^{86}Sr$ being insensitive to the time age correction, increasing by <0.0004 over 750 Ma. Based on the age of the crust and mantle lithosphere in the region, we have calculated initial $^{87}Sr/^{86}Sr$ at 750 Ma. Sixteen samples have initial $^{87}Sr/^{86}Sr$ that range from 0.70257 to 0.70332 (Fig. 5). Two other samples (93719 and 93751-B) have initial $^{87}Sr/^{86}Sr$ of about 0.7049.

The Nd-isotopic data (Table 7) show a wide range of $^{43}Nd/^{144}Nd$, from 0.51257 to 0.51316. This is a wider range than generally displayed by Cenozoic Red Sea rift-related tholeiites and alkali basalts (0.51284–0.51319), although ratios as low as 0.51267 are reported (Altherr et al. 1990). The ε-Nd at 750 Ma ranges from +1 to +7, with a mean of +5.2.

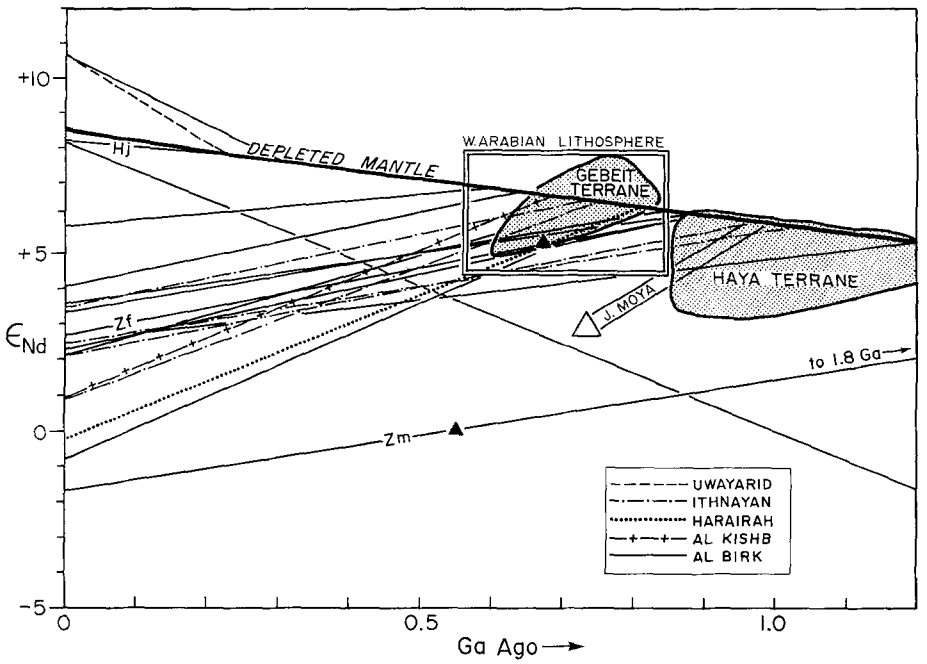

Fig. 6. Nd isotopic data for Arabian granulite xenoliths and model depleted mantle growth curve of Nelson and DePaolo (1985). H_j, Z_m, Z_f as described in Fig. 5. Also shown are the western Arabian lithosphere field of Henjes-Kunst et al. (1990), the field of well-dated samples of upper crust in NE Sudan (Stern and Kröner 1993), the field for the Haya terrane of NE Sudan (Kröner et al. 1991), and Jebel Moya granulites in Sudan (Stern and Dawoud 1991)

Discussion

Thermobarometry

Coexisting mineral assemblages in lower crustal xenoliths can provide information about the temperatures and pressures of last equilibration. In all thermobarometric calculations, all iron was treated as Fe^{2+}. Temperatures from 830 to 980 °C were calculated for the two-pyroxene granulites using the Wells (1977) two-pyroxene thermometer. In the garnet granulites, pyroxenes in coronas surrounding garnet yielded Wells temperatures of 900–1010 °C, and garnet-clinopyroxene temperatures (Ellis and Green 1979) calculated using garnet-clinopyroxene grain center compositions were 930–1,100 °C. The garnet-orthopyroxene barometer of Wood and Banno (1973) yielded pressures of 10 to 12 kbar for the garnet granulites. Pressures cannot be calculated for the two-pyroxene granulite assemblage, but experimental results of Irving (1974) on mafic granulite xenoliths suggest that the two-pyroxene-plagioclase assemblage is stable at 5 to 9 kbar, 800–1,000 °C. This same study also found the stability range of the garnet-clinopyroxene-plagioclase assemblage to be approximately 10 to 20 kbar at temperatures of 900–1,100 °C. These results suggest that the Arabian granulites last equilibrated in the lower crust within a depth range of 15 to 40 km, and the garnet granulites probably originate from greater depth (30–40 km) than the two-pyroxene granulites (15–30 km).

Age

The geologic history of western Saudi Arabia presents two plausible origins for these mafic lower crustal rocks. Following ANS crust formation in the late Proterozoic, the region was tectonically and magmatically quiescent until the initiation of Red Sea rifting approximately 30 million years ago. Therefore, the xenoliths could be samples of lower crust formed contemporaneously with the juvenile upper crust of the ANS in the late Proterozoic, or they may be mafic igneous rocks crystallized from basalts produced during Red Sea rifting in the past 30 million years. Information about the age of these rocks is important in determining their origins and in extrapolating data from these xenoliths to understanding of the formation of the Arabian continental lower crust.

The large spread in geographic location, the presence of obvious variations in initial $^{87}Sr/^{86}Sr$, and the short range in $^{87}Rb/^{86}Sr$ prohibit extraction of age information from the Rb–Sr systematics of these samples. It is noteworthy, however, that the inferred initial $^{87}Sr/^{86}Sr$ observed for the 16 nonradiogenic xenoliths (mean = 0.7030) is very similar to the values observed for lithosphere beneath the Arabian shield, inferred to be ca. 700 Ma (Henjes-Kunst et al. 1990), and for the juvenile upper crust of Afro-Arabia (e.g., Stern and Kröner 1993). We do not know the significance of the two radiogenic samples, but note that ca. 670 Ma felsic granulites from Zabargad Island have even more radiogenic initial $^{87}Sr/^{86}Sr$ (Fig. 5).

Neodymium model ages relative to depleted mantle (T_{DM}, Nelson and DePaolo 1985) range widely from −0.06 to 1.18 Ga (Table 7; Fig. 6). There are several samples with present $^{143}Nd/^{144}Nd$ equal to or greater than that of the depleted mantle model; these yield the negative or < 0.3 Ga model ages. Samson et al. (1991) advocated using only samples with $^{147}Sm/^{144}Nd$ less than 0.16. If we restrict ourselves to such samples, we are left with five T_{DM} model ages in the range 0.68 to 0.81 Ga (mean = 0.76 Ga). If we arbitrarily increase the

cutoff $^{147}Sm/^{144}Nd$ to 0.175, twelve T_{DM} model ages in the range 0.64 to 1.02 Ga are obtained, with a mean age of 0.81 Ga.

There are concerns that T_{DM} model gas ages of mafic cumulates can be interpreted in different ways (Cameron and Robinson 1990; Ruiz et al. 1990). These uncertainties are minimized for the Arabian xenoliths. For the most part, ANS upper crustal igneous rocks fit well with the depleted mantle evolution line of Nelson and DePaolo (1985). Therefore, we assume that the melts in equilibrium with xenoliths also had Nd isotopic compositions that were consistent with this model. Subsequent Nd isotopic evolution would be controlled by the double fractionation of Sm/Nd experienced by the cumulates: first melt-mantle and then cumulate-melt fractionation, but from a geologic perspective both fractionations would be nearly simultaneous. In this case, the T_{DM} model age must approximate the time of fractionation from the mantle. If the xenoliths are residues, interpretation becomes more problematic, but if the difference in time between fractionations is small, as is likely for ANS lower crust, the model may still be useful.

The significance of three samples with $^{147}Sm/^{144}Nd < 0.175$ and Nd-model ages of 0.97 to 1.18 Ga, greater than that of the 900 Ma maximum age of ANS crust, may indicate pre-Pan-African crustal relicts in the ANS lower crust. Alternatively, these may indicate the presence of less-depleted mantle, as argued for the charnockites and enderbites of Jebel Moya in the Sudan (Stern and Dawoud 1991). Reconnaissance geochronologic and Nd-isotopic studies in the Haya terrane of Sudan (Kröner et al. 1991) suggest that slightly less depleted mantle may be an important contributor to the crust of the Haya and Asir terranes. One of the samples (93754) with $^{147}Sm/^{144}Nd < 0.175$ and $T_{TM} > 0.95$ comes from Harrat al Birk, in the Asir terrane. The other two samples (H353-33, H353-34) come from Ithnayn, near the border between the Hijaz and Afif terranes (Fig. 1). Older crust has been documented from the Afif terrane and involvement of such material may be responsible for the older ages from these two Ithnayn xenoliths.

Another way to examine the isotopic data is on a plot of Nd versus Sr isotopic compositions (Fig. 7). It can be seen that while some of the xenoliths have present day Sr and Nd isotopic compositions similar to Cenozoic basalts from the Red Sea and Saudi Arabia, the full range is much greater than that seen in the Cenozoic basalts and even transgresses the mantle array defined by Hart (1988). The data corrected for 750 Ma of radiogenic growth define a field that is much more similar to that of late Precambrian igneous rocks from Saudi Arabia and NE Sudan (Bokhari and Kramers 1981; Duyverman et al. 1982; Stern and Kröner 1993). The data are thus more readily interpreted as indicating a late Precambrian age for the time of formation of these granulites.

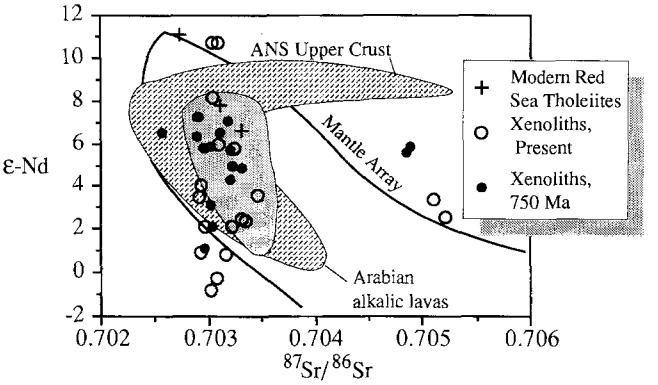

Fig. 7. Plot of ε-Nd versus $^{87}Sr/^{86}Sr$ for Arabian xenoliths. Xenolith data is shown as present isotopic composition, *open circles*, and corrected for 750 Ma of radiogenic growth, *dots*. Also shown is a field for Cenozoic Arabian alkali basalt, analyses for Red Sea tholeiites (Altherr et al. 1990), the mantle array (Hart 1988), and late Precambrian ANS upper crustal rocks (Bokhari and Kramers 1981; Duyverman et al. 1982; Stern and Kröner 1993). Note that the field of ANS upper crustal rocks are initial ratios at 750 Ma, while the mantle array is for present day ratios

Petrogenesis

The granulites are near basaltic in bulk composition. The mineralogy (lack of quartz, corundum, or sillimanite), low Si, Al, Ba, K, Rb, and high Mg, Fe, Ca contents indicate that these are metaigneous granulites and are not metasediments. Geochemical characteristics indicate that most are not basaltic melts. The REE patterns of most of the samples exhibit characteristics of either cumulates formed by fractionation of pyroxene and plagioclase, or mafic residues remaining after partial melting of intermediate rocks to produce felsic melts. All but four of the samples exhibit Eu anomalies, and of those four, only two (H30-82-54 and H332-18) have major element compositions which resemble mafic magma compositions (e.g., BVSP 1981).

Voluminous alkali basalts and their fractionates were erupted on the Saudi Arabian margin of the Red Sea. These basalts carried the granulite xenoliths to the surface, and possible genetic relationships must be considered. Several observations argue against such a relationship. The common occurrence of coexisting clinopyroxene and orthopyroxene in the granulites is not compatible with a cumulate origin from an alkalic basalt at lower crustal pressures (<13 kbar). Olivine is a liquidus phase for alkaline basalt at less than 13 kbar (Presnall et al. 1978), but is not observed in any of the granulites. Nickel and Cr behave as compatible elements in basalts. If these granulites are pyroxene-bearing cumulates or restites, they should have higher Cr contents than their patent liquids. These granulites exhibit lower Ni and Cr than Red Sea rift alkalic or transitional basalts (Fig. 3), suggesting they cannot be related. Barium and Sr are mildly incompatible and should be depleted in cumulates from Red Sea rift basalts. The granulite xenoliths are enriched in Ba and Sr relative to Red Sea basalts. These observations, combined with the isotope systematics, suggests that these granulites are not related to Red Sea rift alkali magmas.

Large volumes of tholeiitic magma (N-MORB and T-MORB; Altherr et al. 1988) have been emplaced along the Red Sea axial trough in the past 5 million

years. Major and trace element data suggest that the granulites are not related to Red Sea tholeiites. The LREE-enriched patterns and positive $(La/Yb)_n$ of many granulites are inconsistent with an origin as cumulates from Red Sea rift N-MORBs or T-MORBs which exhibit flat or LREE-depleted patterns (Altherr et al. 1988). Mafic cumulates from Red Sea MORB should have higher Mg # and Cr contents and lower incompatible element contents, but the granulite xenoliths have lower Mg #, higher Ba and La, and similar Rb contents.

The geochemistry of the granulites is compatible with an origin from island arc calc-alkaline basalts and low-K tholeiites. Similarities to modern island arc basalt suites include the relatively high Al_2O_3 contents (17–20 wt% at 50–55 wt% SiO_2), K_2O contents (0.1–0.9 wt%), average Mg # of 0.58, high K/Rb and Sr/Nd ratios, low Zr, Ti, and Nb contents, and slightly LREE-enriched to flat REE patterns with abundances approximately 10–30 times chondrite. Most trace element (Ni, Cr, Rb, Y, P, V, Zr, Sr, Zn) contents are in the range reported for island arc basalts, but Sc and Cu are lower than typically reported for modern arc basalts (e.g., BVSP 1981). The abundance of modal orthopyroxene and CIPW normative hypersthene is also typical of island arc basalts.

Most samples have compositions indicating mineral fractionation processes. Most have Eu anomalies. Samples H353-33 and H353-34 have 5–10 modal percent Fe–Ti oxides and hence high whole rock TiO_2, FeO, V, Zn and low SiO_2 and K_2O. Sample 93427 is extremely pyroxene rich (approximately 70–80 model percent), resulting in low whole rock contents of Al_2O_3, K_2O, Na_2O, Ba and high MgO, CaO, Sc, Cr, and Ni. The majority of the samples are plagioclase rich with high Al_2O_3, CaO, Na_2O, Sr, and Ba contents, and Eu/Eu* of 1.0 to 2.0.

These geochemical signatures may have been produced by high pressure fractional crystallization of calc-alkaline basalts, or by partial melting of intermediate rocks (tonalites) and extraction of granitic melts leaving mafic restites. Both processes are expected to produce similar characteristics and distinction of cumulates from restites is extremely difficult. Phase relationships suggest that these are more likely cumulates than restites. Partial melting of intermediate rocks should exhaust pyroxene and sodic plagioclase first. Consequently, we expect that restites should be plagioclase rich with calcic plagioclase and positive Eu anomalies. The Arabian granulite xenoliths have relatively sodic plagioclase (An_{27-57}), most exhibit weak Eu anomalies, and several are pyroxene rich (>60%) with negative Eu anomalies (possibly produced by pyroxene accumulation).

Structure of the Arabian continental lower crust

Refraction and gravity studies led Gettings et al. (1986) to infer a mafic bulk composition for the western Arabian lower crust. They modelled a two-layer lower crust with an upper layer from 21 to 29 km depth with seismic velocities (V_p) of 6.60 to 6.75 km/s, and a lower layer

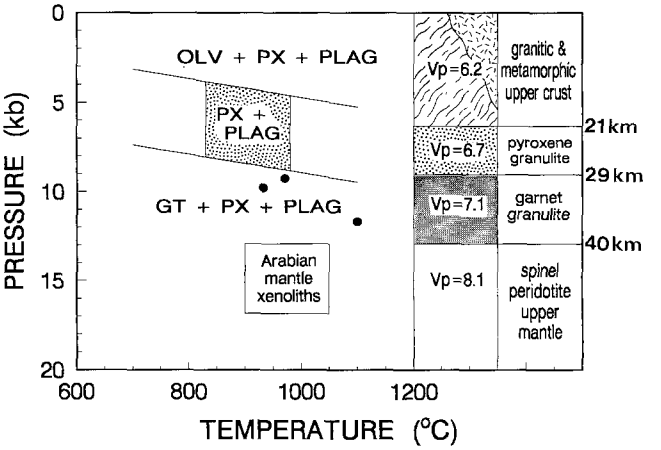

Fig. 8. Estimated temperatures and depths of origin of the granulite xenoliths compared with the crustal model of Gettings et al. (1986) derived from geophysical data.Two-pyroxene granulites fall in pyroxene+plagioclase, *stippled PX+PLAG*, field, and garnet granulite *T–P* estimates are shown by *dots*. Reaction boundaries of olivine granulite to pyroxene granulite to garnet granulite from Irving (1974); *T–P* range of Arabian upper mantle xenoliths from McGuire (1988)

from 29 to about 40 km depth with seismic velocities of 7.18 to 7.29 km/s. Predicted depths and seismic velocities of our granulite xenoliths are in accord with this model (Fig. 8). Thermobarometric calculations discussed above indicate possible depths of 15–30 km for the two-pyroxene granulites and 30–40 km for the garnet granulites. Seismic velocities were estimated for the granulites using the model proportions of plagioclase, pyroxene and garnet, and the graphical method of Christensen and Fountain (1975). Estimated V_p are 6.6 to 7.6 for the two-pyroxene granulites, with values greater than 7.0 due to high model pyroxene in some samples, and 7.0 to 7.6 for the garnet granulites. We suggest that the Arabian lower crust consists of a dominantly two pyroxene granulite upper layer from about 21 to 29 km depth, and a dominantly garnet granulite±pyroxenite lower layer from about 29 to 40 km depth.

Composition of the Arabian continental lower crust

The Arabian granulite xenoliths were collected from localities as much as 1000 km apart, yet are very similar in lithology and composition. This widespread geographic distribution of similar lithologies, in combination with good agreement with the geophysical models of the Arabian lower crust (Gettings et al. 1986), leads us to propose that these granulites are reasonably representative of the Arabian lower continental crust. The similarity of the Arabian xenoliths to lower crustal granulite xenoliths from northern Israel (Mittlefehldt 1983) further supports the suggestion that the Arabian continental lower crust is dominated by mafic, metaigneous granulite. We recognize the fact that xenolith suites are often unrepresentative of the complete crust-mantle section through which they have been transported; however, we believe that the geophysical and geologic constraints in this case validate our acceptance of this xeno-

Table 8. Average Arabian lower crustal composition

	Average	Weighted average
Major elements (wt%)		
SiO_2	50.3	49.3
TiO_2	1.0	0.9
Al_2O_3	16.5	16.0
FeO	9.1	9.6
MnO	0.2	0.2
MgO	7.1	7.9
CaO	10.2	10.5
Na_2O	3.3	3.0
K_2O	0.4	0.3
P_2O_5	0.2	0.1
Total	98.3	97.8
Mg #	0.58	0.59
Trace and rare earth elements (ppm)		
P	940	720
Sc	29	32
V	260	270
Cr	250	470
Ni	80	74
Cu	36	42
Zn	91	88
Ga	16	16
Rb	1.72	1.63
Sr	610	560
Y	16	17
Zr	49	48
Nb	2.7	2.5
Ba	190	160
Pb	0.5	0.5
Th	0.5	0.6
La	5.3	4.4
Ce	14	12
Nd	10	9.2
Sm	2.8	2.7
Eu	1.0	1.0
Gd	2.9	3.0
Yb	1.4	1.6

Average, average composition of 18 xenoliths; weighted average, composition of 50% average two-pyroxene granulite plus 50% average garnet granulite

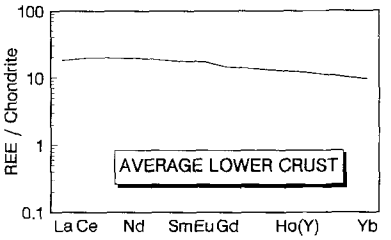

Fig. 9. REE pattern for average lower crustal granulite composition

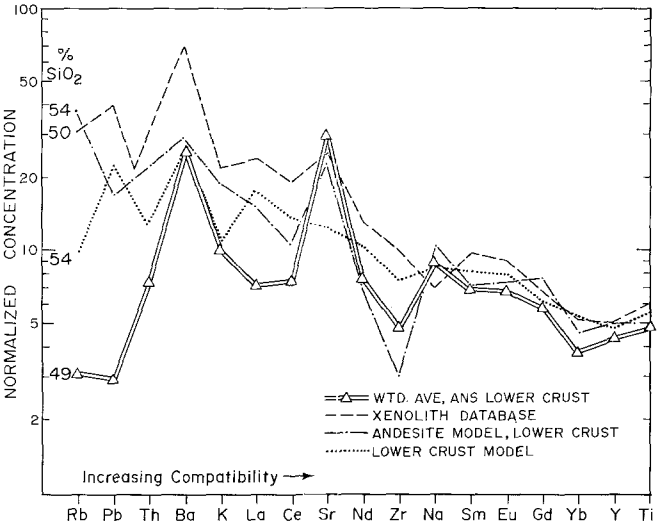

Fig. 10. Elemental compatibility diagram for weighted average Arabian lower crust and other estimates for the lower crust (xenolith database, Kempton et al. 1990; andesite model lower crust, Weaver and Tarney 1980; model lower crust, Taylor and McClennan 1985). Elemental compatibility for continental crust increase to the *right*. Normalization is to the primitive mantle of Hofmann (1988)

lith suite as a *reasonable approximation* of the Arabian lower crust.

We can calculate an average Arabian lower crustal composition, assuming that granulite xenoliths are representative of the lower crust (Table 8). We have calculated the average of 18 xenolith whole rock compositions (14 two-pyroxene granulites and 4 garnet granulites). The geophysical data suggest that proportions of two-pyroxene granulite to garnet granulite may be more equal; therefore we have calculated a weighted average composition of 50% average two-pyroxene granulite plus 50% average garnet granulite compositions. The two compositions are similar.

The calculated Arabian lower crust average composition is mafic (50 wt% SiO_2), and similar to calc-alkaline basalts found in oceanic island arc settings. The REE pattern (Fig. 9) is slightly LREE enriched with concentrations about ten times chondrite and a slight positive Eu anomaly. Barium and Sr are enriched relative to MORB, and Zr, Nb, Ti, Cu, Ni, and (heavy) REE are depleted relative to MORB. Compared to other estimates of lower crustal compositions (Fig. 10), the ANS lower crust is markedly lower in silica and elements that are more incompatible than Zr, with the possible exceptions of Ba and Sr. With the exception of these 'spikes', elemental abundances are remarkably constant at about seven times primitive mantle. Estimated abundance of strongly incompatible elements in the ANS lower crust are about 10 to 30% of the abundances in other estimated lower crustal compositions. We find particularly strong depletions in Rb, supporting inferences of high K/Rb in low-K granulites (Rudnick et al. 1985).

At present, good estimates of average ANS upper crustal composition are not available. Studies of Arabian Precambrian upper crustal rocks suggest that they are dominantly felsic and intermediate composition volcanic and plutonic igneous and metaigneous rocks (e.g., Bokhari and Kramers 1981; Marzouki et al. 1982; and others). The combination of a mafic lower crust with a felsic upper crust would suggest an intermediate, possibly andesitic, bulk crustal composition, similar to the average post-Archean continental crust proposed by

Taylor and McLennan (1985). If the Arabian upper crust is more intermediate in composition, then the bulk crustal composition will be more mafic than the andesitic model of Taylor and McLennan and closer to the mafic crustal compositions calculated by Pearcy et al. (1990) for crust generated in island arcs. Estimates of the composition of mantle-derived, juvenile continental crust formed in island arcs may need to be adjusted towards a more mafic basalt or basaltic andesite model composition.

Formation of the Arabian continental lower crust

The xenolith data reported here, in conjunction with the geophysical data, depict a remarkably homogeneous, mafic lower crust beneath the ANS. This is important because there is little control on the composition of the lower crust in young orogens; that is, in regions where plate tectonic processes can be demonstrated to have formed the continental crust. The lower crust formed beneath intra-oceanic arcs is mafic (Takahashi 1978; Kay and Kay 1985; DeBari and Coleman 1989; Pearcy et al. 1990). Some authors have suggested that the lower crust beneath Archean cratons is markedly more felsic (e.g., Durrheim and Mooney 1991). Because all modifications to the lower crust accompanying melting and underplating must make the lower crust increasingly mafic, there is no way to make felsic lower crust from mafic lower crust. The implication is that modern plate tectonic processes forming the lower crust are fundamentally different than those that made Archean lower crust. The perspective gained from our data for lower crust of the ANS is especially valuable because this clearly is an example of plate tectonics generating juvenile continental crust.

There are three major models for generating mafic lower crust:

1. Melting of andesitic bulk crust to generate felsic upper crust and mafic restite lower crust. This is the "internal differentiation" of Ben Othman et al. (1984).
2. Basaltic underplating as a result rift-related igneous activity (White and McKenzie 1989).
3. Fractional crystallization of mafic magmas to form thick cumulate sections beneath juvenile, intra-oceanic arcs.

All three processes can operate either prior to or following terrane accretion. Whereas it is widely accepted that arcs comprise the fundamental architectural elements of the continental crust (at least for as long as plate tectonics has controlled lithospheric evolution), it is becoming increasingly apparent that basaltic and not andesitic melts are what is delivered from the mantle to the base of the crust at convergent margins (Kay and Kay 1985; Pearcy et al. 1990). Insofar as the bulk continental crust is made up of juvenile arcs, it must also be basaltic. Internal differentiation of this crust can generate only a very thin felsic upper crust, not the ca. 29 km thickness characteristic of Proterozoic and younger upper crust (Durrheim and Mooney 1991). This consideration makes possibility no. 1 unlikely.

Distinguishing between possibilities nos. 2 and 3 is more difficult and must rely on the tectonic affinities of the xenoliths inferred from geochemistry and the constraints placed by observed upper crustal geology. Although the Arabian granulites are not related to Cenozoic Red Sea rift basalts, as discussed above, it is possible that a late Precambrian rift event occurred in the region. Geochemical characteristics of the Arabian xenoliths support possibility no. 3. Both Ba and La are highly incompatible and Ba/La will approximate that of the equilibrium liquid. The Ba/La value in the calculated average ANS lower crust is about 35, similar to that expected for arc magmas and higher than expected for MORB or OIB (20–50 vs <10; Stern et al. 1989) and considerably higher than that of Cenozoic Arabian basalts (ca. 10; Coleman et al. 1983). The Ba/Zr value is about 3.3, significantly higher than typical for OIB or MORB (<1.4) and similar to that for juvenile arcs such as the Marianas (2–5; Woodhead 1989). However, Ce/Pb is about 28, similar to that of MORB (25; Hofmann 1988) and OIB (14–38; Sun and McDonough 1989) and distinctly higher than typical for arcs (ca. 2–4; Kay 1980). Consideration of the normalized element plot (Fig. 10) also sheds some light on this problem. Depletions in Zr are observed, providing support for a model of arc-related lower crustal formation. The spike in Sr may reflect sequestering in plagioclase, but the Ba enrichment suggests an arc component. On the whole, the elemental patterns observed in Fig. 10 support an origin at a convergent margin for the Arabian granulites. In summary, the trace element data are most consistent with an origin of the ANS lower crust as a result of igneous activity at one or more convergent margins. Whether most of this growth occurred before or after terrane accretion can not be sorted out at present.

Conclusions

Extensive work on upper crustal rocks of western Arabia and eastern Egypt and Sudan (Stoeser and Camp 1985; Vail 1985; and others) has shown that the upper crust in this region formed by accretion of island arc terranes during the late Proterozoic. Data from the Saudi Arabian lower crustal xenolith suite suggest that the lower crust of this region formed in the same setting and contemporaneously with formation of the upper crust in a convergent margin setting.

Although the Saudi Arabian granulite xenolith suite should not be treated as a co-magmatic suite, the samples are similar in lithology and composition. Most appear to have formed as cumulates from island arc basalts. Studies of lower crustal rocks from modern island arcs and older arc terranes indicate that mafic cumulates may form in the lower crust of arcs. We envision a similar origin for the Arabian lower continental crust. Fractionation of mantle-derived magmas to produce large amounts of mafic cumulates should also have produced significant volumes of intermediate and felsic composition magmas. These may now be represented as plutonic and volcanic rocks forming the Arabian upper continen-

tal crust. Partial melting of juvenile crust may also have produced mafic restites in the lower crust.

There is excellent correlation between published geophysical models (Gettings et al. 1986) and predicted seismic velocities and depths of origin for the granulite xenoliths. The widespread distribution of similar rock types and similarity to lower crustal granulite xenoliths in northern Israel suggests that these samples are representative of the Arabian lower crust. Average lower crustal composition is mafic, and bulk Arabian continental composition is predicted to be intermediate to mafic depending on estimates of upper crustal composition.

The xenolith isotopic data indicate the Arabian lower crust formed entirely from mantle-derived material. These data, and lack of metasedimentary xenoliths, agree with studies of upper crustal rocks which conclude that there are no indications of older sialic continental crust involved in formation of the western Arabian-Nubian continental crust.

Acknowledgements. The authors wish to thank Bob Coleman and the National Museum of Natural Sciences, Smithsonian Institution, for the loan of samples. The sample preparation efforts of Ron Nhim and Trung Nguyen were appreciated. David Mittlefehldt and Joaquin Ruiz reviewed the manuscript. A.V.M. acknowledges support from NSF grant EAR-9005414, and R.J.S. acknowledges support from NSF grant OCE-8918481.

References

Abdelsalam MG, Stern RJ (1992) Tectonic evolution of the Nakasib suture Red Sea Hills, Sudan: evidence for a Wilson cycle in the late Precambrian of the Arabian-Nubian Shield. J Geol Soc London (in press)

Albee AL, Ray AL (1970) Correction factors for electron probe microanalysis of silicates, oxides, carbonates, phosphates, and sulfates. Anal Chem 42:1408–1414

Altherr R, Henjes-Kunst F, Puchelt H, Baumann A (1988) Volcanic activity in the Red Sea axial trough – evidence for a large mantle diapir? Tectonophysics 150:121–133

Altherr R, Henjes-Kunst F, Baumann A (1990) Asthenosphere versus lithosphere as possible sources for basaltic magmas erupted during formation of the Red Sea: constraints from Sr, Pb and Nd isotopes. Earth Planet Sci Lett 96:269–286

Basaltic Volcanism Study Project (BVSP) (1981) Basaltic volcanism on the terrestrial planets. Pergamon Press, New York

Ben Othman D, Polvé M, Allègre CJ (1984) Nd-Sr isotopic composition of granulites and constraints on the evolution of the lower continental crust. Nature 307:510–515

Bokhari FY, Kramers JD (1981) Island arc character and late Precambrian age of volcanics at Wadi Shwas, Hijaz, Saudi Arabia: geochemical and Sr and Nd isotopic evidence. Earth Planet Sci Lett 54:409–422

Bonatti E, Seyler M (1987) Crustal underplating and evolution in the Red Sea rift: uplifted gabbro/gneiss crustal complexes on Zabargad and Brothers Islands. J Geophys Res 92:12803–12821

Boudier F, Nicolas A, Ji S, Kienast JR, Mevel C (1988) The gneiss of Zabargad Island: deep crust of a rift. Tectonophysics 150:209–227

Cameron KL, Robinson JV (1990) Comments on "Comments on Nd-Sr isotopic compositions of lower crustal xenoliths – evidence for the origin of mid-Tertiary felsic volcanics in Mexico" by J Ruiz, PJ Patchett, and RJ Arculus. Contrib Mineral Petrol 104:609–614

Camp VE, Roobol MJ (1989) The Arabian continental alkali basalt province. I. Evolution of Harrat Rahat, Kingdom of Saudi Arabia. Geol Soc Am Bull 101:71–95

Christensen NI, Fountain DM (1975) Constitution of the lower continental crust based on experimental studies of seismic velocities in granulite. Geol Soc Am Bull 86:227–236

Coleman RG, Gregory RT, Brown GF (1983) Cenozoic volcanic rocks of Saudi Arabia. US Geol Surv Open-File Rep USGS-OF-03-93

DeBari SM, Coleman RG (1989) Examination of the deep levels of an island arc: evidence from the Tonsina ultramafic-mafic assemblage, Tonsina, Alaska. J Geophys Res 94:4373–4391

Durrheim RJ, Mooney WD (1991) Archean and Proterozoic crustal evolution: evidence from crustal seismology. Geology 19:606–609

Duyverman HJ, Harris NBW, Hawkesworth CJ (1982) Crustal accretion in the Pan African: Nd and Sr isotopic evidence from the Arabian shield. Earth Planet Sci Lett 59:315–326

Ellis DJ, Green DH (1979) An experimental study of the effect of Ca upon garnet-clinopyroxene Fe–Mg exchange equilibria. Contrib Mineral Petrol 71:13–22

Esperança S, Garfunkel Z (1986) Ultramafic xenoliths from the Mt. Carmel area (Karem Maharal Volcano), Israel. Lithos 19:43–49

Gettings ME, Blank HR, Mooney WD, Healey JH (1986) Crustal structure of southwestern Saudi Arabia. J Geophys Res 91:6491–6512

Ghent ED, Coleman RG, Hadley DG (1980) Ultramafic inclusions and host alkali olivine basalts of the southern coastal plain of the Red Sea, Saudi Arabia. Am J Sci 280-A:499–527

Harris NBW, Gass IG, Hawkesworth CJ (1990) A geochemical approach to allochthonous terranes: a Pan-African case study. Philos Trans R Soc London A 331:533–548

Hart SR (1988) Heterogeneous mantle domains: signatures, genesis and mixing chronologies. Earth Planet Sci Lett 90:273–296

Henjes-Kunst F, Altherr R, Baumann A (1990) Evolution and composition of the lithospheric mantle underneath the western Arabian peninsula: constraints from Sr–Nd isotope systematics of mantle xenoliths. Contrib Mineral Petrol 105:460–472

Hofmann AW (1988) Chemical differentiation of the Earth: the relationship between mantle, continental crust, and oceanic crust. Earth Planet Sci Lett 90:297–314

Irving AJ (1974) Geochemical and high pressure experimental studies of garnet pyroxenite and pyroxene granulite xenoliths from the Delegate basaltic pipes, Australia. J Petrol 15:1–40

Kay RW (1980) Volcanic arc magmas: implications of a melting-mixing model for element recycling in the crust-upper mantle system. J Geol 88:497–522

Kay SM, Kay RW (1985) Role of crystal cumulates and the oceanic crust in the formation of the lower crust of the Aleutian arc. Geology 13:461–464

Kempton PD, Harmon RS, Hawkesworth CJ, Moorbath S (1990) Petrology and geochemistry of lower crustal granulites from the Geronimo Volcanic Field, southeastern Arizona. Geochim Cosmochim Acta 54:3401–3426

Krogh TE (1973) A low-contamination method for hydrothermal decomposition of zircon and extraction of U and Pb for isotopic age determinations. Geochim Cosmochim Acta 37:485–494

Kröner A, Linnebacher P, Stern RJ, Reischmann T, Manton W, Hussein IM (1991) Evolution of Pan-African island arc assemblages in the southern Red Sea Hills, Sudan, and in southwestern Arabia as exemplified by geochemistry and geochronology. Precambrian Res 53:99–118

Lancelot JR, Bosch D (1991) A Pan-African age for the H*P*-H*T* granulite geneisses of Zabargad island: implications for the early stages of the Red Sea rifting. Earth Planet Sci Lett 107:539–549

Leyreloup A, Bodinier. JL, Dupuy C, Dostal J (1982) Petrology and geochemistry of granulite xenoliths from Central Hoggar (Algeria) – implications for the lower crust. Contrib Mineral Petrol 79:68–75

Lin P-N, Stern RJ, Bloomer SH (1989) Shoshonitic volcanism in the northern Mariana arc. 2. Large-ion lithophile and rare earth element abundances: evidence for the source of incompatible element enrichments in intraoceanic arcs. J Geophys Res 94:4497–4514

Lin P-N, Stern RJ, Morris J, Bloomer SH (1990) Nd- and Sr-isotopic composition of lavas from the northern Mariana and southern Volcano arcs: implications for the origin of island arc melts. Contrib Mineral Petrol 105:381–392

Marzouki FMH, Jackson NJ, Ramsay CR (1982) Composition, age and origin of two Proterozoic diorite-tonalite complexes in the Arabian shield. Precambrian Res 19:31–50

McGuire AV (1988) The mantle beneath the Red Sea margin: xenoliths from western Saudi Arabia. Tectonophysics 150:101–119

Mittlefehldt DW (1983) The lower crust of northern Israel. Isr Geol Soc Annu Meet 1983, pp 58–59

Mittlefehldt DW (1986) Petrology of high pressure clinopyroxenite series xenoliths, Mount Carmel, Israel. Contrib Mineral Petrol 94:245–252

Nelson BK, DePaolo DJ (1985) Rapid production of continental crust 1.7 to 1.9 billion years ago: Nd isotopic evidence from the basement of the North American midcontinent. Geol Soc Am Bull 96:746–754

Norman MD, Leeman WP, Blanchard DP, Fitton JG, James D (1989) Comparison of major and trace element analyses by ICP, XRF, INAA, and ID methods. Geostandards News 13:283–290

Pearcy LG, De Bari SM, Sleep NH (1990) Mass balance calculations for two sections of island arc crust and implications for the formation of continents. Earth Planet Sci Lett 96:427–442

Pier JG, Podosek FA, Luhr JF, Brannon JC, Aranda-Gómez JJ (1989) Spinel-lherozolite-bearing Quaternary volcanic centers in San Luis Potosi, Mexico. 2. Sr and Nd isotopic systematics. J Geophys Res 94:7941–7951

Presnall DC, Dixon SA, Dixon JR, O'Donnell TH, Brenner NL, Schrock RL, Dycus DW (1978) Liquidus phase relations on the join diopside-forsterite-anorthite from 1 atm to 20 kbar: their bearing on the generation and crystallization of basaltic magma. Contrib Mineral Petrol 66:203–220

Rudnick RL, McLennan SM, Taylor SR (1985) Large ion lithophile elements in rocks from high-pressure granulite facies terrains. Geochim Cosmochim Acta 49:1645–1655

Ruiz J, Patchett P, Arculus RJ (1990) Reply to "Comments on Nd–Sr isotopic compositions of lower crustal xenoliths – evidence for the origin of mid-Tertiary felsic volcanics in Mexico" by KL Cameron and JV Robinson. Contrib Mineral Petrol 104:615–618

Samson SD, Patchett PJ, McClelland WC, Gehrels GE (1991) Nd isotopic characterization of metamorphic rocks in the Coast Mountains, Alaska and Canadian Cordillera: ancient crust bounded by juvenile terranes. Tectonics 10:770–780

Seyler M, Bonatti E (1988) Petrology of a gneiss-amphibolite lower crustal unit from Zabargad Island, Red Sea. Tectonophysics 150:177–207

Stern RJ, Dawoud AS (1991) Late Precambrian (740 Ma) charnockite, enderbite, and granite from Jebel Moya, Sudan: a link between the Mozambique belt and the Arabian-Nubian Shield. J Geol 99:648–659

Stern RJ, Kröner A (1993) Geochronologic and isotopic constraints on late Precambrian crustal evolution in NE Sudan (in press)

Stern RJ, Bloomer SH, Lin P-N, Smoot NC (1989) Submarine arc volcanism in the southern Mariana arc as an ophiolite analogue. Tectonophysics 168:151–170

Stern RJ, Lin P-N, Morris J, Jackson MC, Fryer P, Bloomer SH, Ito E (1990) Enriched back-arc basin basalts from the northern Mariana Trough: implications for the magmatic evolution of back-arc basins. Earth Planet Sci Lett 100:210–225

Stoeser DB, Camp VE (1985) Pan-African microplate accretion of the Arabian shield. Geol Soc Am Bull 96:817–826

Sun S-S, McDonough WF (1989) Chemical and isotopic systematics of oceanic basalts: implications for mantle compositions and processes. In: Saunders AD, Norry MJ (eds) Magmatism in the ocean basins. Geol Soc London Spec Publ 42, pp 313–345

Takahashi E (1978) Petrologic model of the crust and upper mantle of the Japanese island arcs. Bull Volcanol 41:531–547

Taylor SR (1967) The origin and growth of continents. Tectonophysics 4:17–34

Taylor SR, McClennan SM (1985) The continental crust: its composition and evolution. Blackwell, Oxford, U.K.

Vail JR (1985) Pan-African (late Precambrian) tectonic terrains and the reconstruction of the Arabian-Nubian Shield. Geology 13:839–842

Weaver BL, Tarney J (1980) Continental crust composition and nature of the lower crust: constraints from mantle Nd–Sr isotope correlation. Nature 286:342–346

Wells PRA (1977) Pyroxene geothermometry in simple and complex systems. Contrib Mineral Petrol 62:129–139

White R, McKenzie D (1989) Magmatism at rift zones: the generation of volcanic continental margins and flood basalts. J Geophys Res 94:7685–7729

Wood BJ, Banno S (1973) Garnet-orthopyroxene and orthopyroxene-clinopyroxene relationships in simple and complex systems. Contrib Mineral Petrol 42:109–124

Woodhead JD (1989) Geochemistry of the Mariana arc (western Pacific): source composition and processes. Chem Geol 76:1–24